Hierarchical follow-up of subthreshold candidates of an all-sky Einstein@Home search for continuous gravitational waves on LIGO sixth science run data

Maria Alessandra Papa,[1,2,4,*] Heinz-Bernd Eggenstein,[2,3] Sinéad Walsh,[1,2] Irene Di Palma,[1,2,5] Bruce Allen,[2,4,3] Pia Astone,[5] Oliver Bock,[2,3] Teviet D. Creighton,[7] David Keitel,[2,3,6] Bernd Machenschalk,[2,3] Reinhard Prix,[2,3] Xavier Siemens,[4] Avneet Singh,[1,2,3] Sylvia J. Zhu,[1,2] and Bernard F. Schutz[8,1]

[1]*Max-Planck-Institut für Gravitationsphysik, am Mühlenberg 1, 14476 Potsdam, Germany*
[2]*Max-Planck-Institut für Gravitationsphysik, Callinstraße 38, 30167 Hannover, Germany*
[3]*Leibniz Universität Hannover, Welfengarten 1, 30167 Hannover, Germany*
[4]*University of Wisconsin-Milwaukee, Milwaukee, Wisconsin 53201, USA*
[5]*Universita di Roma "La Sapienza," P.zle A. Moro 2, 00185 Roma, Italy*
[6]*Universitat de les Illes Balears, IAC3—IEEC, E-07122 Palma de Mallorca, Spain*
[7]*The University of Texas Rio Grande Valley, Brownsville, Texas 78520, USA*
[8]*Cardiff University, Cardiff CF24 3AA, United Kingdom*

(Received 1 September 2016; published 28 December 2016)

We report results of an all-sky search for periodic gravitational waves with frequency between 50 and 510 Hz from isolated compact objects, e.g., neutron stars. A new hierarchical multistage approach is taken, supported by the computing power of the Einstein@Home project, allowing us to probe more deeply than ever before. 16 million subthreshold candidates from the initial search [LIGO Scientific and Virgo Collaborations, Phys. Rev. D **94**, 102002 (2016)] are followed up in four stages. None of those candidates is consistent with an isolated gravitational wave emitter, and 90% confidence level upper limits are placed on the amplitudes of continuous waves from the target population. Between 170.5 and 171 Hz, we set the most constraining 90% confidence upper limit on the strain amplitude h_0 at 4.3×10^{-25}, while at the high end of our frequency range, we achieve an upper limit of 7.6×10^{-25}. These are the most constraining all-sky upper limits to date and constrain the ellipticity of rotating compact objects emitting at 300 Hz at a distance D to less than 6×10^{-7} $[\frac{D}{100\ \mathrm{pc}}]$.

DOI: 10.1103/PhysRevD.94.122006

I. INTRODUCTION

The beauty of continuous signals is that, even if a candidate is not significant enough to be recognized as a real signal after a first semicoherent search, it is still possible to improve its significance to the level necessary to claim a detection after a series of follow-up searches. Hierarchical approaches were first proposed in the late 1990s and developed over a number of searches on LIGO data: Refs. [1] and [2] detail a semicoherent search plus a three-stage follow-up of order 100 candidates; Refs. [3] and [4] detail a semicoherent search plus a series of vetoes and a final coherent follow-up of over 1000 candidates. The search detailed here follows up 16 million candidates and is the first large-scale hierarchical search ever done.

We use a hierarchical approach consisting of four stages applied to the processed results ("Stage 0") of an initial search [5]. At each stage, a semicoherent search is performed, and the top ranking cells in parameter space (also referred to as "candidates") are marked and are searched in the next stage. At each stage, the significance of a cell harboring a real signal would increase with respect to the significance it had in the previous stage. The significance of a cell that did not contain a signal, on the other hand, is not expected to increase consistently over the different stages. In the first three stages, the thresholds that define the top ranking cells are low enough that many false alarms are expected over the large parameter space that was searched. And indeed at the end of the first stage, we have 16 million candidates. At the end of the second stage, we have five million. At the end of the third stage, we have one million. At the end of the fourth stage we are left with only 10 candidates.

The paper is organized very simply. Section II introduces the quantities that characterize each stage of the follow-up. Section III illustrates how the different stages were set up and the results for the S6 LIGO Einstein@Home candidates follow-ups. Section IV present the gravitational wave amplitude and ellipticity upper limit results. In the last section, Sec. V, we summarize the main findings and discuss prospects for this type of search.

*maria.alessandra.papa@aei.mpg.de

II. QUANTITIES DEFINING EACH STAGE

From one stage to the next in this hierarchical scheme, the number of surviving candidates is reduced, the uncertainty over the signal parameters for each candidate is also reduced, and the significance of a real signal is increased. This latter effect is due both to the search being intrinsically more sensitive and to the trials' factor decreasing for every search from one stage to the next.

Each stage performs a stack-slide type of search using the Global Correlations Transform (GCT) method and implementation of Refs. [6,7]. Important variables are the coherent time baseline of the segments, the number of segments used ($N_{\rm seg}$), the total time spanned by the data, the grids in parameter space, and the detection statistic used to rank the parameter space cells. All stages use the same data set. The first three follow-up searches are performed on the Einstein@Home volunteer computing platform [8], and the last is performed on the Atlas computing cluster [9].

The parameters for the various stages are summarized in Table I. The grids in frequency and spindown are each described by a single parameter, the grid spacing, which is constant over the search range. The same frequency grid spacings (δf) are used for the coherent searches over the segments and for the incoherent summing. The spindown spacing for the incoherent summing step is finer than that ($\delta \dot{f}_c$) used for the coherent searches by a factor γ. The notation used here is consistent with that used in previous observational papers [3,5,10] and in the GCT methods papers [6,7].

The sky grids for stages 1 to 4 are approximately uniform on the celestial sphere projected on the ecliptic plane. The tiling is a hexagonal covering of the unit circle with hexagons' edge length d,

$$d(m_{\rm sky}) = \frac{1}{f}\frac{\sqrt{m_{\rm sky}}}{\pi\tau_E}, \tag{1}$$

with $\tau_E \simeq 0.021$ s being half of the light travel time across the Earth and $m_{\rm sky}$ the so-called mismatch parameter. As was done in previous searches [1,5], the sky grids are constant over 10 Hz bands, and the spacings are the ones associated through Eq. (1) to the highest frequency in the range. The sky grid of stage 0 is the union of two grids: one is uniform on the celestial sphere after projection onto the equatorial plane, and the tiling (in the equatorial plane) is approximately square with edge $d(0.3)$ from Eq. (1); the other grid is limited to the equatorial region ($0 \le \alpha \le 2\pi$ and $-0.5 \le \delta \le 0.5$), with constant actual α and δ spacings equal to $d(0.3)$ (see Fig. 1 of Ref. [5]). The reason for the equatorial "patching" with a denser sky grid is to improve the sensitivity of the search.

After each stage, a threshold is set on the detection statistic to determine what candidates will be searched by the next stage. We set this detection threshold to be the highest such that the weakest signal that survived the first stage of the pipeline would, with high confidence, not be lost.

The setup for each stage is determined at fixed computational cost. The computational cost is mostly set by practical considerations such as the time frame on which we would like to have a result, the number of stages that we envision in the hierarchy, and the availability of Einstein@Home.

Since an analytical model that predicts the sensitivity of a search with the current implementation of the GCT method does not exist, we consider different search setups, and for every setup we perform fake-signal injection and recovery Monte Carlos. From these, we determine the detection efficiency and the signal parameter uncertainty for signals at the detection threshold. We pick the search setup based on these. Typically, the search setup with the lowest parameter uncertainty volume also has the highest detection efficiency, and we pick that. As a further cross-check, we also determine the mismatch distributions for the detection statistic. We define the mismatch μ as

$$\mu = \frac{2\overline{\mathcal{F}}_{\rm signal} - 2\overline{\mathcal{F}}_{\rm candidate}}{2\overline{\mathcal{F}}_{\rm signal} - 4}, \tag{2}$$

where $\overline{\mathcal{F}}_{\rm signal}$ is the value of the detection statistic that we measure when we search the data with a template that is perfectly matched to the signal and $\overline{\mathcal{F}}_{\rm candidate}$ is the value of the detection statistic that we obtain when running a search on a set of templates, none of which, in general, will perfectly coincide with the signal waveform. The mismatch is hence a measure of how fine the grid that we are using is. As expected, Fig. 1 shows that the grids of subsequent stages get finer and finer.

At each stage, we determine the signal parameter uncertainty for signals at least at the detection threshold, in each search dimension: the distance in parameter space

TABLE I. Search parameters for each of the semicoherent stages.

	$T_{\rm coh}$ (hr)	$N_{\rm seg}$	δf (Hz)	$\delta \dot{f}_c$ (Hz/s)	γ	$m_{\rm sky}$
Stage 0	60	90	1.6×10^{-6}	5.8×10^{-11}	230	0.3 + equatorial patch
Stage 1	60	90	3.6×10^{-6}	1×10^{-10}	230	0.0042
Stage 2	140	44	2.0×10^{-6}	2.4×10^{-11}	100	0.0004
Stage 3	140	44	1.8×10^{-6}	2.1×10^{-11}	100	1×10^{-5}
Stage 4	280	22	1.9×10^{-7}	7.0×10^{-12}	50	4×10^{-7}

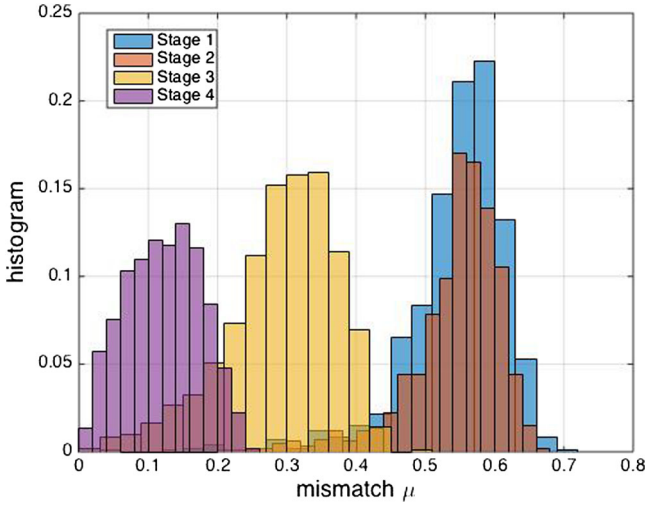

FIG. 1. These are the mismatch histograms of the four follow-up searches, so the y axis represents normalized counts. For a given search and search setup, the mismatch distribution depends on the template grid. The injection-and-recovery Monte Carlo studies to determine these distributions were performed without noise.

around a candidate that with high confidence (at least 90%) includes the signal parameter values. The uncertainty region around each candidate associated with stage i is searched in stage $i+1$. The uncertainty volume at stage i is smaller than the uncertainty volume of stage $i-1$.

III. S6 SEARCH FOLLOW-UP

A series of all-sky Einstein@Home searches looked for signals with frequencies from 50 through 510 Hz and frequency derivatives from 3.1×10^{-10} through -2.6×10^{-9} Hz/s. Results from these were combined and analyzed as described in Ref. [5]: no significant candidate was found, and upper limits were set on the gravitational wave signal amplitude in the target signal parameter space. The data set that we begin with is that described in Secs. III. 1 and III. 2 of Ref. [5]: a ranked list of 3.8×10^{10} candidates, each with an associated detection statistic value $2\overline{\mathcal{F}}$. We now take the 16 million most promising regions in parameter space from that search and inspect them more closely. This is done in four stages, which we describe in the next subsections.

We remind the reader that some of the input data to this search were treated by substituting the original frequency-domain data with fake Gaussian noise at the same level as that of the neighboring frequencies. This is done in frequency regions affected by well-known artifacts, as described in Ref. [5]. Results stemming entirely from these fake data are not considered in any further stage. Moreover, after the initial Einstein@Home search, the results in 50 mHz bands were visually inspected, and those 50 mHz bands that presented obvious noise disturbances were also removed from the analysis. A complete list of the excluded bands is given in the Appendixes of Ref. [5]. We will come back to this point as we present the results of this search.

A. Stage 0

This is the most complex stage of the hierarchy and determines the sensitivity of the search; if a signal does not pass this initial stage, it will be lost. So, we try here to keep the threshold that candidates have to exceed to be considered further as low as possible, compatibly with the feasibility of the next stage with the available computing resources. Such a threshold was set at $2\overline{\mathcal{F}}=6.109$.

The identification of correlated candidates saves compute cycles in the next steps of the search. As was done in Ref. [3], the clustering procedure aims to bundle together candidates that could be ascribed to the same cause. In fact, a loud signal as well as a loud disturbance would produce high values of the detection statistic at a number of different template grid points, and it would be a waste to follow up each of these independently. As described in Refs., [3,4], we begin with the loudest candidate, i.e., the candidate with the highest value of $2\overline{\mathcal{F}}$. This is the seed for the first cluster. We associate with it close-by candidates in parameter space. Together, the seed and the nearby candidates constitute the first cluster. We remove the candidates from the first cluster from the candidate list. The loudest candidate on the resulting list is the seed of the second cluster. We proceed in the same way as for the first cluster and reiterate the procedure until no more seeds with $2\overline{\mathcal{F}}$ values equal to or larger than 6.109 remain.

Monte Carlo studies are conducted to determine the cluster box size, i.e., the neighborhood of the seed that determines the cluster occupants. We inject signals in Gaussian noise data at the level of our detectors' noise, search a small parameter space region around the signal parameters, and use the resulting candidates as a representative of what we would find in an actual search. For signals at the detection threshold, the 90% confidence cluster box is

$$\begin{cases} \Delta f^{\text{Stage-0}} & = \pm 1.2\times10^{-3}\ \text{Hz} \\ \Delta \dot{f}^{\text{Stage-0}} & = \pm 2.6\times10^{-10}\ \text{Hz/s} \\ \Delta\text{sky}^{\text{Stage-0}} & \simeq 25\ \text{points around seed.} \end{cases} \quad (3)$$

If we consider as cluster occupants only those with $2\overline{\mathcal{F}}$ values greater than or equal to 5.9, we observe that signals tend to produce slight overdensities in the clusters with respect to noise. This feature is exploited with an *occupancy veto* that discards all clusters with less than two occupants. We find that the false dismissal for signals at threshold is hardly affected (∼0.02% of signal clusters), whereas the noise rejection is quite significant: we exclude 45% of noise clusters.

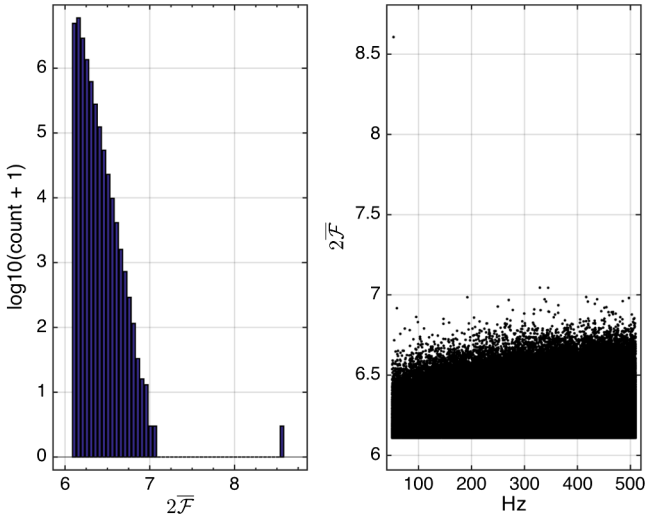

FIG. 2. Candidates that are followed up in Stage-1: the distribution of their detection statistic values $2\bar{\mathcal{F}}$ (left plot) and their distribution as a function of frequency (right plot). Most notable are two outliers around ≈ 53 Hz close enough in frequency that they are not resolvable in the left plot.

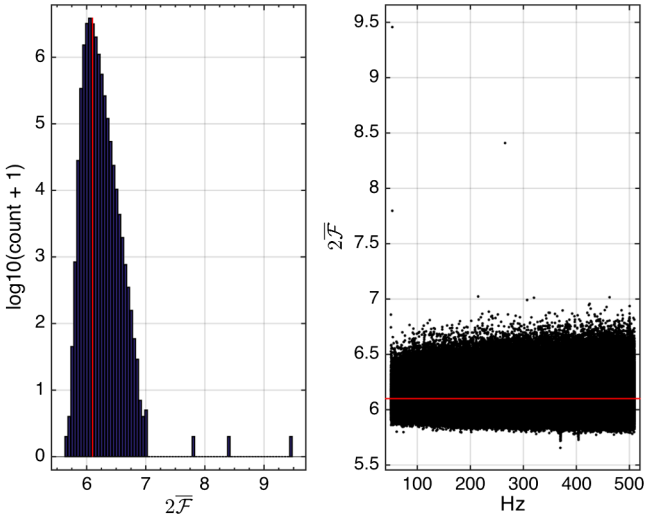

FIG. 3. Loudest from each of the Stage-1 searches: the distribution of their detection statistic values $2\overline{\mathcal{F}}$ (left plot) and their distribution as a function of frequency (right plot). The red line marks $2\bar{\mathcal{F}} = 6.109$, which is the threshold at and above which candidates are passed on to stage 2. The two outliers at ≈53 Hz also visible in the previous stage remain notable, and another one becomes visible, at ≈266 Hz.

This same data set containing fake signals is utilized to characterize the false dismissals and the parameter uncertainty regions for all the stages of the hierarchy.

To summarize, the total number of candidates returned by the Einstein@Home searches is 3.8×10^{10}. Of these, we consider the ones with $2\overline{\mathcal{F}}$ above 6.109, excluding frequency bands with obvious noise disturbances. There are 21.6 million such candidates. After clustering and occupancy veto, we reduced this number to 16.23×10^6. The distribution of the detection statistic values $2\overline{\mathcal{F}}$ for these candidates is shown in Fig. 2 as is their distribution in frequency. The maximum value is 8.6 and occurs at ≈ 53 Hz. All remaining values are smaller than 7.1.

B. Stage 1

In this stage we search a volume of parameter space around each candidate (around each seed) equal to the cluster box defined by Eq. (3). We fix the total run time to be 4 months on Einstein@Home, and this yields an optimal search set-up having the same coherent time baseline as stage 0, 60 h, with the same number of segments $N_{\text{seg}} = 90$ and the grid spacings shown in Table I. We use the same ranking statistic as in the original search [5], the $\hat{O}_{\text{SGL}}$ [11], with the same tunings (c_* and normalized short Fourier transform power threshold). The 90% uncertainty regions for this search setup for signals just above the detection threshold are

$$\begin{cases} \Delta f^{\text{Stage-1}} & = \pm 6.7 \times 10^{-4}\ \text{Hz} \\ \Delta \dot{f}^{\text{Stage-1}} & = \pm 1.8 \times 10^{-10}\ \text{Hz/s} \\ \Delta\text{sky}^{\text{Stage-1}} & \simeq 0.55\, \Delta\text{sky}^{\text{Stage-0}}. \end{cases} \tag{4}$$

The search is divided among 16.23×10^6 work units (WUs), each lasting about 2 h and performed by one of the Einstein@Home volunteer computers. From each follow-up search, we record the most significant candidate. The distribution of these is shown in Fig. 3. A threshold at $2\overline{\mathcal{F}} = 6.109$ has a ∼9% false dismissal for signals at threshold (Fig. 4) and a 70% noise rejection. Using this threshold to determine what candidates to consider in the next stage yields 5.3×10^6 candidates.

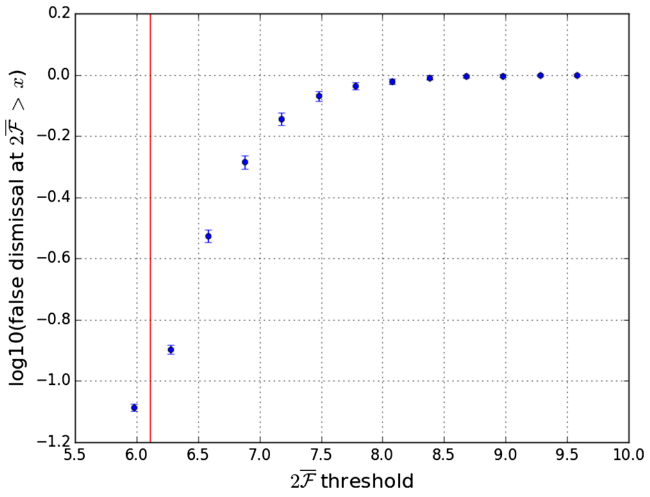

FIG. 4. Fraction of signals that are recovered with a detection statistic value larger than or equal to the threshold value after the Stage-1 follow-up.

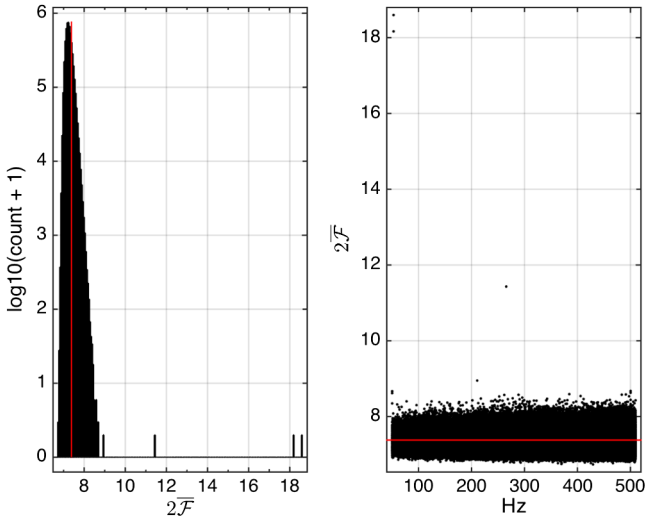

FIG. 5. Loudest from each of the Stage-2 searches: the distribution of their detection statistic values $2\bar{\mathcal{F}}$ (left plot) and their distribution as a function of frequency (right plot). The red line marks $2\bar{\mathcal{F}} = 7.38$, which is the threshold at and above which candidates are passed on to stage 3. The two outliers at ≈53 Hz and the one at ≈266 Hz from the previous stage remain significant. A new candidate stands out of the bulk of the distribution at ≈220 Hz, and two new candidates begin to appear at ≈50 Hz.

C. Stage 2

In this stage, we search a volume of parameter space around each candidate defined by Eq. (4). As shown in Table I, we use a coherent time baseline which is about twice as long as that used in the previous stages and the grid spacings are finer. The ranking statistic is $\hat{O}_{\mathrm{SGL}}$ with the same tunings (c_* and normalized short Fourier transform power threshold) as in the previous stages. The computational load is divided among 5.3×10^6 WUs, each lasting about 12 h.

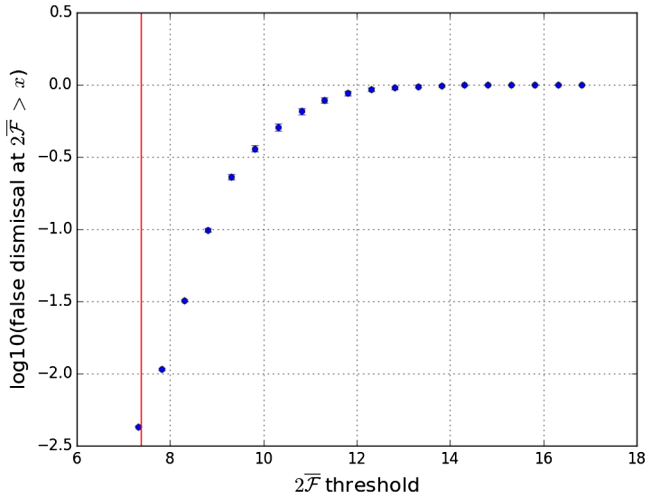

FIG. 6. Fraction of signals that are recovered with a detection statistic value larger than or equal to the threshold value after the Stage-2 follow-up.

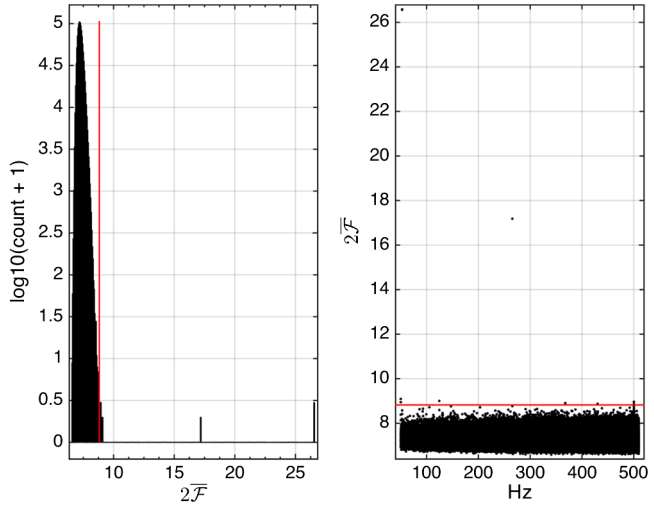

FIG. 7. Loudest from each of the Stage-3 searches: the distribution of their detection statistic values $2\bar{\mathcal{F}}$ (left plot) and their distribution as a function of frequency (right plot). The red line marks $2\bar{\mathcal{F}} = 8.82$, which is the threshold at and above which candidates are passed on to stage 4. The two outliers at ≈53 Hz and the one at ≈266 Hz well visible in all the previous stages remain significant; these are the ones that are clearly outside of the bulk of the distribution. The candidate that at Stage-2 was at ≈220 Hz has now fallen below threshold, whereas the two at ≈50 Hz have risen above threshold. Five new candidates have emerged just above threshold.

The $> 99\%$ uncertainty regions for this search setup for signals close to the detection threshold are

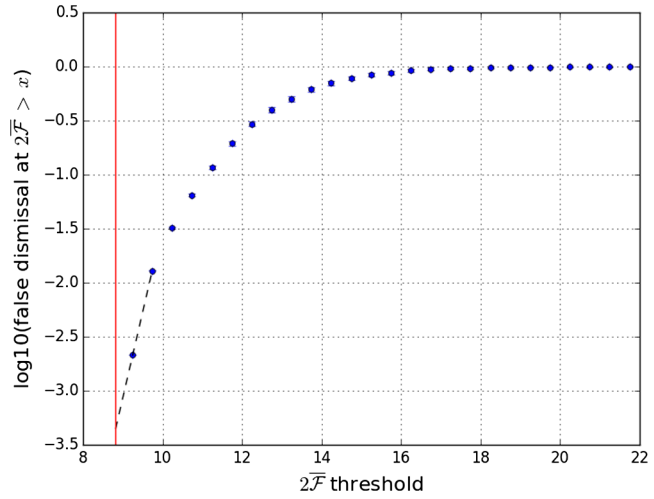

FIG. 8. Fraction of signals that are recovered with a detection statistic value larger than or equal to the threshold value (vertical line) after the Stage-3 follow-up. The dashed line is a linear extrapolation based on the last two data points to guide the eye to the false dismissal value for signals at threshold. This line is a conservative estimate in the sense that it overestimates the false dismissal.

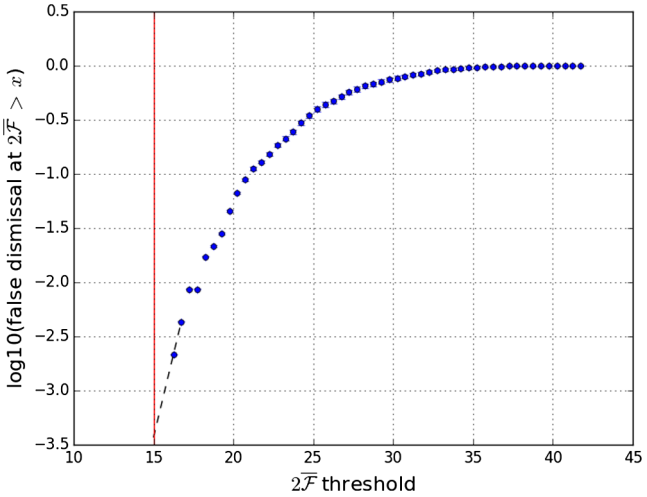

FIG. 9. Fraction of signals that are recovered with a detection statistic value larger than or equal to the threshold value (vertical line) after the Stage-4 follow-up. The dashed line is a linear extrapolation based on the last two data points to guide the eye to the false dismissal value for signals at threshold. This line is a conservative estimate in the sense that it overestimates the false dismissal.

$$\begin{cases} \Delta f^{\text{Stage-2}} & = \pm 1.9 \times 10^{-4}\ \text{Hz} \\ \Delta \dot{f}^{\text{Stage-2}} & = \pm 3.5 \times 10^{-11}\ \text{Hz/s} \\ \Delta\text{sky}^{\text{Stage-2}} & \simeq 0.19\, \Delta\text{sky}^{\text{Stage-1}}. \end{cases} \quad (5)$$

As was done in stage 1, we record the most significant candidate from each search. The distribution is shown in Fig. 5. In the next stage, we follow up the top 1.1 million candidates, corresponding to a threshold on $2\overline{\mathcal{F}}$ at 7.38. This threshold has a ∼0.6% false dismissal for signals at threshold (Fig. 6) and a 79% noise rejection.

D. Stage 3

In this stage, we search a volume of parameter space around each candidate defined by Eq. (5). As shown in Table I, the coherent time baseline is as long as that used in the previous stage, but the grid spacings are finer. The search is divided among 1.1 million WUs, each lasting about 2 h.

The >99% uncertainty regions for this search setup for signals close to the detection threshold are

$$\begin{cases} \Delta f^{\text{Stage-3}} & = \pm 5 \times 10^{-5}\ \text{Hz} \\ \Delta \dot{f}^{\text{Stage-3}} & = \pm 7 \times 10^{-12}\ \text{Hz/s} \\ \Delta\text{sky}^{\text{Stage-3}} & \simeq 0.4\, \Delta\text{sky}^{\text{Stage-2}}. \end{cases} \quad (6)$$

As was done in previous stages, we record the most significant candidate from each search. The distribution is shown in Fig. 7. In the next stage, we follow up the top ten candidates, corresponding to a threshold on $2\overline{\mathcal{F}}$ at 8.82.

TABLE II. Stage-4 results from each of the ten follow-ups from the candidates surviving Stage-3. For illustration purposes, in the last two columns, we show the values of the average single-detector detection statistics. Typically, for signals, the single-detector values do not exceed the multidetector $2\bar{\mathcal{F}}$.

ID	f (Hz)	α (rad)	δ (rad)	$\dot{f}$ (Hz/s)	$2\bar{\mathcal{F}}$	$2\bar{\mathcal{F}}_{\text{H1}}$	$2\bar{\mathcal{F}}_{\text{L1}}$
1	50.19985463	4.7716026	1.1412922	3.013×10^{-11}	11.6	6.9	9.5
2	50.20001612	4.7124554	1.1683832	-5.674×10^{-12}	12.3	5.5	11.2
3	52.80832455	5.2805366	−1.4631895	7.311×10^{-14}	52.0	16.9	39.7
4	52.80832422	5.2819543	−1.4632398	2.968×10^{-14}	55.9	18.1	44.0
5	124.60002077	4.7067880	1.1648704	-4.164×10^{-12}	11.8	11.2	6.1
6	265.57623841	1.2487972	−0.9812202	-4.015×10^{-12}	37.3	25.1	17.0
7	367.83543941	1.4807437	0.7112582	-9.236×10^{-10}	10.4	9.5	4.9
8	430.28626637	6.1499768	0.9203753	-2.056×10^{-9}	10.0	7.3	5.5
9	500.36312713	4.7121294	1.1617860	9.878×10^{-13}	12.2	11.9	5.4
10	500.36594568	4.5662765	1.4276343	-2.507×10^{-9}	10.6	10.0	4.6

TABLE III. Columns 2–6 show the parameters of the fake injected signal closest to the candidate whose ID identifies it in Table II. The reference time (GPS s) is 960541454.5. We note that the h_0 upper limit values for the 0.5 Hz bands corresponding to the frequencies of these recovered fake signals are consistent with the fake signals' amplitudes. Columns 7–9 display the distance between the candidates' and the signals' parameters (candidate parameter minus signal parameter).

ID	f_s (Hz)	α_s (rad)	δ_s (rad)	$\dot{f}_s$ (Hz/s)	h_0	Δf (Hz)	$\Delta\alpha$ (rad)	$\Delta\delta$ (rad)	$\Delta\dot{f}$ (Hz/s)
3	52.8083244	5.281831296	−1.463269033	-4.03×10^{-18}	4.85×10^{-24}	1.5×10^{-7}	-1.29×10^{-3}	7.95×10^{-5}	7.3×10^{-14}
4	52.8083244	5.281831296	−1.463269033	-4.03×10^{-18}	4.85×10^{-24}	-1.8×10^{-7}	1.23×10^{-4}	2.92×10^{-5}	3.0×10^{-14}
6	265.5762386	1.248816734	−0.981180225	-4.15×10^{-12}	2.47×10^{-25}	-1.9×10^{-7}	-1.95×10^{-5}	-4.00×10^{-5}	1.4×10^{-13}

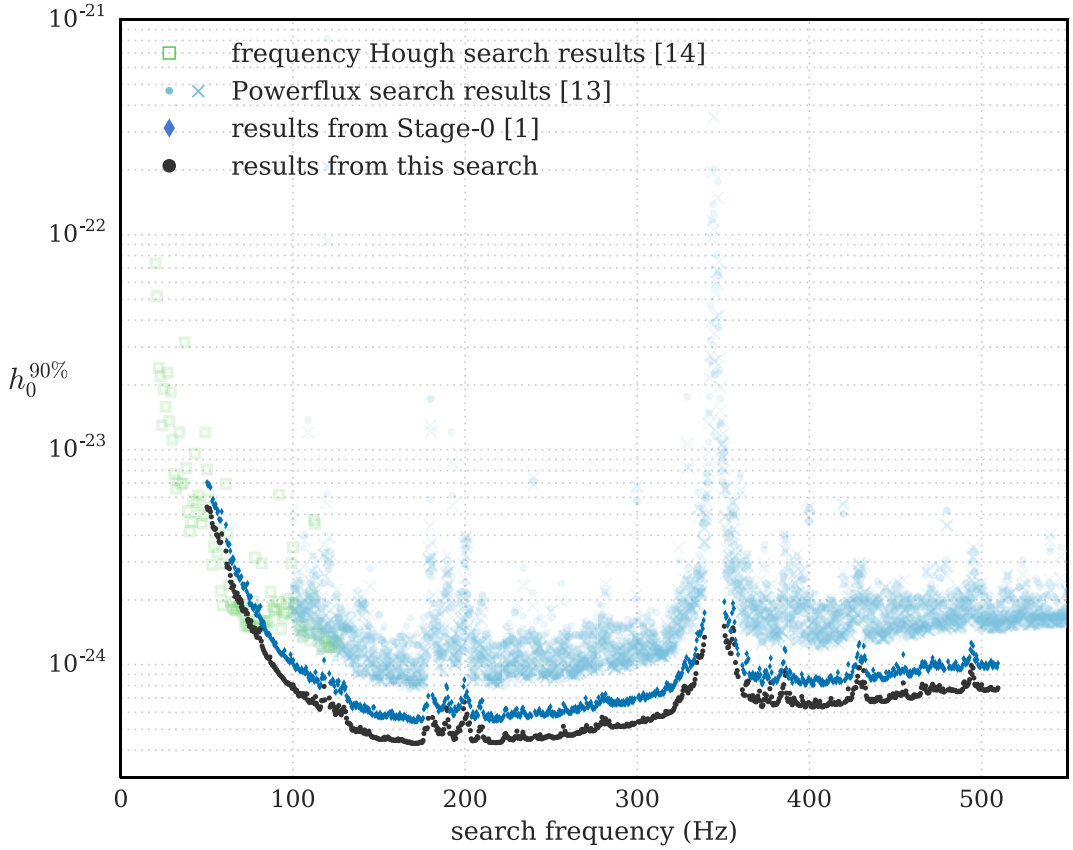

FIG. 10. 90% confidence upper limits on the gravitational wave amplitude of continuous gravitational wave signals with frequency in 0.5 Hz bands and with spindown values within the searched range. The lowest set of points (black circles) is the result of this search. For comparison, we show the upper limits from only the stage-0 results [5]. These lie on the curve above the lowest one and are marked by dark blue diamonds. The results from a previous broad all-sky survey [13] are the top curve (lighter circles and crosses) above 100 Hz. In the lower frequency range, we compare with a search on Virgo data contemporary to the LIGO S6 data [14].

This threshold has a $\sim 4 \times 10^{-4}$ false dismissal for signals at threshold (Fig. 8) and a 99.9991% noise rejection.

E. Stage 4

In this stage, we search a volume of parameter space around each candidate defined by Eq. (6). The setup of choice has a coherent time baseline of 280 h, twice as long as that used in stage 3, and the grid spacings shown in Table I. The search has a relatively modest cost and is performed on the Atlas cluster: each follow-up lasts about 14 h. The ranking statistic is $\hat{O}_{\mathrm{SGL}}$ with a retuned $c_* = 96.1$. We consider the loudest candidate from each of the ten follow-ups. In our Monte Carlo studies, no signal candidate (out of 464 injections at threshold) was found more distant than

$$\begin{cases} \Delta f^{\text{Stage-4}} & = \pm 4 \times 10^{-7}\ \text{Hz} \\ \Delta \dot{f}^{\text{Stage-4}} & = \pm 4.0 \times 10^{-13}\ \text{Hz/s} \\ \Delta\text{sky}^{\text{Stage-4}} & \simeq 0.03\, \Delta\text{sky}^{\text{Stage-3}}. \end{cases} \quad (7)$$

None of those injections has a $2\overline{\mathcal{F}}$ below 16.2 (Fig. 9), so conservatively, we pick a threshold at 15.0. The Gaussian false alarm at $2\overline{\mathcal{F}} = 15.0$ for a search over the volume of Eq. (6) is very low ($\approx 2 \times 10^{-20}$), and hence we do not expect any candidate from random Gaussian noise fluctuations.

Since we only follow up ten candidates, we report our findings explicitly for each follow-up. As was done in the previous stages, we consider the most significant candidate from each follow-up. Table II details each of these candidates. Only candidates 3, 4, and 6 have a detection statistic value above the detection threshold $2\overline{\mathcal{F}} = 15.0$, but unfortunately they are ascribable to fake signals hardware injected in the detector to test the detection pipelines. The search recovers all fake signals in the data with parameters within its search range and not absurdly loud.[1] We note that

[1]A fake signal was injected at about 108 Hz at such a high amplitude that it saturates the Einstein@Home toplists across the entire sky. Upon visual inspection, it is immediately obvious that the $f - \dot{f}$ morphology is that of a signal, albeit an unrealistically loud one. We categorized the associated band as disturbed because the data are corrupted by this loud injection and it is impossible to detect any real signal in its frequency neighborhood.

candidates 3 and 4 come from the same fake signal. For a complete list of the fake signals present in the data, see Table 6 of Ref. [12]. In Table III, we show the signal parameters and report the distance with respect to the candidate parameter values. These distances are all within the stage-4 uncertainties of Eq. (7). We do not follow up these candidates any further because we know that they are associated with the hardware injections.

The remaining candidates are below the threshold of 15.0, which is the minimum value of $2\overline{\mathcal{F}}$ that we demand candidates to pass before we inspect them further. However, since these are the most significant ten candidates out of 16 million, we have all the same considered each of them, and it is worth spending a few words on them. Candidates 1 and 2 are close in frequency and are very likely due to the same root cause. The frequencies are also very close to being exact multiples of 0.1 Hz, which is a known comb of spectral artifacts, and the positions are close to the ecliptic poles, which is where stationary lines in the detector frame aggregate in the search results. The same considerations also apply to candidate 5. Candidates 9 and 10 are similar to candidates 1 and 2, apart from the fact that the frequencies are not close to multiples of 0.1 Hz. However, these candidates come from a spectral region where we see an excess of noise candidates. Candidates 7 and 8 cannot be ruled out based on the arguments made previously, so we dug deeper. In particular, we looked at the per-segment contributions to the average detection statistic. We did not find that all segments contribute consistently, as would be expected for a signal. Furthermore, the per-segment detection statistic does not grow as expected between the third- and fourth-stage follow-up. This makes it very unlikely that these candidates come from a continuous gravitational wave signal, phase coherent during the observational period.

IV. RESULTS

The search did not reveal any continuous gravitational wave signal in the parameter volume that was searched. We hence set frequentist upper limits on the maximum gravitational wave amplitude consistent with this null result in 0.5 Hz bands: $h_0^{90\%}(\mathrm{f})$. $h_0^{90\%}(\mathrm{f})$ is the GW amplitude such that 90% of a population of signals with parameter values in our search range would have been detected by our search, i.e., would have survived the last $2\overline{\mathcal{F}}$ threshold at 15.0 at stage 4. Since an actual full-scale injection-and-recovery Monte Carlo for the entire set of follow-ups in every 0.5 Hz band is prohibitive, in the same spirit as Refs. [5,10], we perform such a study in a limited set of trial bands. We pick 100. For each of these, we determine the sensitivity depth of the search corresponding to the detection criterion stated above. As representative of the sensitivity depth $\mathcal{D}^{90\%}$ of this hierarchical search, we take the average of these depths, 46.9 $[1/\sqrt{\mathrm{Hz}}]$. Given the noise level of the data as a function of frequency, $S_h(f)$, we then determine the 90% upper limits as

$$h_0^{90\%}(f) = \frac{\sqrt{S_h(f)}}{\mathcal{D}^{90\%}}. \tag{8}$$

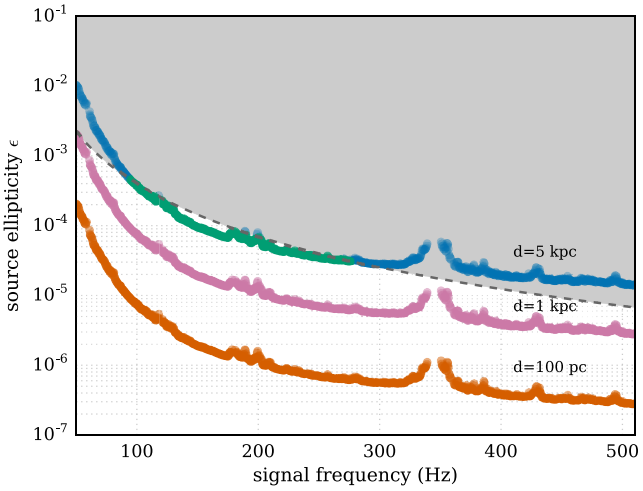

FIG. 11. Ellipticity ϵ of a source at a distance d emitting continuous gravitational waves that would have been detected by this search. The dashed line shows the spindown ellipticity for the highest magnitude spindown parameter value searched: 2.6×10^{-9} Hz/s. The spindown ellipticity is the ellipticity necessary for all the lost rotational kinetic energy to be emitted in gravitational waves. If we assume that the observed spindown is all actual spindown of the object, then no ellipticities could be possible above the dashed curve. In reality, the observed and actual spindowns could differ due to radial motion of the source. In this case, the actual spindown of the object may even be larger than the apparent one. In this case, our search would be sensitive to objects with ellipticities above the dashed line.

Figure 10 shows these upper limits as a function of frequency. They are also presented in tabular form in Table IV in the Appendix with the associated uncertainties, which amount to 20%, including calibration uncertainties. The most constraining upper limit is in the band between 170.5 and 171 Hz, and it is 4.3×10^{-25}. At the upper end of the frequency range, around 510 Hz, the upper limit rises to 7.6×10^{-25}.

The upper limits can be recast as exclusion regions in the signal frequency-ellipticity plane parametrized by the distance, for an isolated source emitting continuous gravitational waves due to its shape presenting an ellipticity ϵ,

$$\epsilon = \frac{|I_{xx} - I_{yy}|}{I_{zz}}, \tag{9}$$

where I are the principal moments of inertia and the coordinate system is taken so that the z axis is aligned with the spin axis of the star. Figure 11 shows these upper

limits. Above 200 Hz, we can exclude sources with ellipticities larger than 10^{-6} within 100 pc of Earth and above 400 Hz ellipticities above 4×10^{-7}, values that are much lower than the highest ones that compact objects could sustain [15].

V. CONCLUSIONS

With a hierarchy of five semicoherent searches at increasing coherent time baselines and resolutions in parameter space, we searched over 16 million regions over a few hundred Hz around the most sensitive frequencies of the LIGO detectors during the S6 science run. All stages but the very last ran on the Einstein@Home distributed computing project, lasting a few to several weeks. This is the first large-scale hierarchical search for gravitational wave signals ever performed.

Having carried out this search proves that one can successfully perform deep follow-ups of marginal candidates and elevate their significance to the level necessary to be able to claim a detection. This paper proves that searches with thresholds at the level of the Einstein@Home search described in Ref. [16] are possible; Ref. [16] demonstrates that they are the most sensitive, and these observational results confirm this.

The sensitivity of broad surveys for continuous gravitational wave signals is computationally limited. For this reason, we employ Einstein@Home to deploy our searches. However, following up tens of millions of candidates is not just a matter of having the computational power. This paper illustrates how to perform and optimize the different stages, factoring in all the practical aspects of a real analysis.

None of the investigated candidates survived the five stages, apart from those arising from the two fake signals injected in the detector for control purposes. These fake signals were recovered with the correct signal parameters. Candidate 6 comes from a hardware injection weak enough that no other search on this data set was ever able to detect it. This search recovers it well above the detection threshold.

The gravitational wave amplitude upper limits that we set improve on existing ones [5] by about 30%. This corresponds to an increase in accessible space volume of $\simeq 2$.

We excluded 10% of the original data from this analysis where the Stage-0 results had different statistical properties than the bulk of the results and the automated methods employed here, which are necessary in order to deal with a large number of candidates, would not have yielded meaningful statistical results. We might go back to these excluded parameter space regions and attempt to extract information. This is a time-consuming process, and the odds of finding a signal vs the odds of missing one by not analyzing more sensitive data might well indicate that we should not pursue this.

The optimal setup for the various stages and the upper limits were determined at the expense of signal injection-and-recovery Monte Carlo studies. This is due to the fact that the implementation of a stack-slide search that we are using does not allow an analytical prediction of the sensitivity of a search with a given setup (coherent segments and grid spacings). This major drawback will soon be overcome by a new implementation of stack-slide searches based on Refs. [17–20]. Such a search is being characterized and tuned at the time of writing, and we hope to employ it in the context of our contributions to the LIGO Scientific Collaboration for searches on data from the O2 LIGO run.

In principle, we would like to carry out the entire hierarchy of stages on Einstein@Home. For this to happen, two aspects of the search presented here need to be automated: the visual inspection and the follow-up stages. The first is underway [21]. The second will be significantly eased by the new stack-slide search to which we alluded, above.

ACKNOWLEDGMENTS

Our sincere gratitude first goes to the Einstein@Home volunteers who have made these searches possible. Maria Alessandra Papa, Sinéad Walsh, Bruce Allen, and Xavier Siemens gratefully acknowledge the support from NSF PHY Grant No. 1104902. The work for this paper was funded by the Max-Planck-Institut für Gravitationsphysik and the Leibniz Universität Hannover (Germany), the Italian Istituto Nazionale di Fisica Nucleare and the Universita' di Roma La Sapienza, Rome (Italy), The University of Texas, Rio Grande Valley, Brownsville, Texas (USA) and Cardiff University, Cardiff (UK). All the tuning and preparatory computational work for this search was carried out on the ATLAS supercomputing cluster at the Max-Planck-Institut für Gravitationsphysik/Leibniz Universität Hannover. We also acknowledge the Continuous Wave Group of the LIGO Scientific Collaboration for useful discussions and Graham Woan for reviewing the manuscript on behalf of the collaboration. This document has been assigned LIGO Laboratory document number LIGO-P1600213.

APPENDIX: TABULAR DATA

1. Upper limit values

TABLE IV. First frequency of each half Hz signal frequency band in which we set upper limits and the upper limit value for that band.

f (Hz)	$h_0^{90\%} \times 10^{25}$	f (Hz)	$h_0^{90\%} \times 10^{25}$	f (Hz)	$h_0^{90\%} \times 10^{25}$	f (Hz)	$h_0^{90\%} \times 10^{25}$
50.063	54.1 ± 10.8	50.563	52.6 ± 10.5	51.063	53.3 ± 10.7	51.563	53.2 ± 10.6
52.063	51.5 ± 10.3	52.563	48.7 ± 9.7	53.063	45.4 ± 9.1	53.563	43.5 ± 8.7
54.063	43.5 ± 8.7	54.563	42.5 ± 8.5	55.063	42.9 ± 8.6	55.563	40.2 ± 8.0
56.063	40.1 ± 8.0	56.563	39.1 ± 7.8	57.063	37.4 ± 7.5	57.563	36.9 ± 7.4
58.063	37.1 ± 7.4	58.563	40.6 ± 8.1	61.063	33.8 ± 6.8	61.563	29.5 ± 5.9
62.063	28.8 ± 5.8	62.563	28.4 ± 5.7	63.063	27.9 ± 5.6	63.563	26.0 ± 5.2
64.063	24.1 ± 4.8	64.563	22.9 ± 4.6	65.063	22.8 ± 4.6	65.563	23.2 ± 4.6
66.063	21.8 ± 4.4	66.563	20.9 ± 4.2	67.063	20.9 ± 4.2	67.563	21.5 ± 4.3
68.063	20.3 ± 4.1	68.563	20.6 ± 4.1	69.063	19.6 ± 3.9	69.563	20.1 ± 4.0
70.063	19.4 ± 3.9	70.563	18.6 ± 3.7	71.063	17.9 ± 3.6	71.563	17.8 ± 3.6
72.063	17.8 ± 3.6	72.563	17.9 ± 3.6	73.063	17.3 ± 3.5	73.563	17.3 ± 3.5
74.063	16.2 ± 3.2	74.563	15.9 ± 3.2	75.063	15.2 ± 3.0	75.563	16.0 ± 3.2
76.063	15.0 ± 3.0	76.563	14.4 ± 2.9	77.063	14.3 ± 2.9	77.563	14.2 ± 2.8
78.063	14.8 ± 3.0	78.563	13.7 ± 2.7	79.063	13.4 ± 2.7	79.563	14.3 ± 2.9
80.063	14.2 ± 2.8	80.563	13.3 ± 2.7	81.063	14.7 ± 2.9	81.563	12.9 ± 2.6
82.063	12.2 ± 2.4	82.563	11.9 ± 2.4	83.063	11.6 ± 2.3	83.563	11.3 ± 2.3
84.063	11.2 ± 2.2	84.563	11.0 ± 2.2	85.063	10.8 ± 2.2	85.563	10.8 ± 2.2
86.063	10.7 ± 2.1	86.563	10.9 ± 2.2	87.063	10.2 ± 2.0	87.563	10.1 ± 2.0
88.063	9.9 ± 2.0	88.563	10.0 ± 2.0	89.063	9.7 ± 1.9	89.563	9.7 ± 1.9
90.063	9.5 ± 1.9	90.563	9.4 ± 1.9	91.063	9.3 ± 1.9	91.563	9.2 ± 1.8
92.063	9.0 ± 1.8	92.563	8.9 ± 1.8	93.063	8.8 ± 1.8	93.563	8.8 ± 1.8
94.063	8.7 ± 1.7	94.563	8.6 ± 1.7	95.063	8.5 ± 1.7	95.563	8.3 ± 1.7
96.063	8.3 ± 1.7	96.563	8.2 ± 1.6	97.063	8.2 ± 1.6	97.563	8.1 ± 1.6
98.063	8.1 ± 1.6	98.563	8.1 ± 1.6	99.063	7.9 ± 1.6	99.563	7.8 ± 1.6
100.063	8.1 ± 1.6	100.563	7.8 ± 1.6	101.063	7.7 ± 1.5	101.563	7.5 ± 1.5
102.063	7.6 ± 1.5	102.563	7.4 ± 1.5	103.063	7.2 ± 1.4	103.563	7.1 ± 1.4
104.063	7.2 ± 1.4	104.563	7.3 ± 1.5	105.063	7.2 ± 1.4	105.563	7.1 ± 1.4
106.063	7.3 ± 1.5	106.563	7.1 ± 1.4	107.063	7.0 ± 1.4	107.563	7.3 ± 1.5
108.063	7.3 ± 1.5	108.563	6.8 ± 1.4	109.063	6.8 ± 1.4	109.563	6.7 ± 1.3
110.063	6.7 ± 1.3	110.563	6.7 ± 1.3	111.063	6.8 ± 1.4	111.563	6.9 ± 1.4
112.063	6.7 ± 1.3	112.563	6.6 ± 1.3	113.063	7.1 ± 1.4	113.563	6.6 ± 1.3
114.063	6.4 ± 1.3	114.563	6.4 ± 1.3	115.063	6.3 ± 1.3	115.563	6.2 ± 1.2
116.063	6.4 ± 1.3	116.563	6.8 ± 1.4	117.063	6.8 ± 1.4	117.563	6.8 ± 1.4
118.063	7.9 ± 1.6	118.563	6.9 ± 1.4	121.063	7.0 ± 1.4	121.563	6.3 ± 1.3
122.063	6.5 ± 1.3	122.563	6.5 ± 1.3	123.063	6.6 ± 1.3	123.563	6.4 ± 1.3
124.063	6.1 ± 1.2	124.563	5.9 ± 1.2	125.063	5.9 ± 1.2	125.563	6.3 ± 1.3
126.063	6.1 ± 1.2	126.563	6.5 ± 1.3	127.063	6.0 ± 1.2	127.563	6.0 ± 1.2
128.063	5.8 ± 1.2	128.563	6.2 ± 1.2	129.063	6.1 ± 1.2	129.563	6.3 ± 1.3
130.063	6.0 ± 1.2	130.563	6.1 ± 1.2	131.063	5.6 ± 1.1	131.563	5.4 ± 1.1
132.063	5.4 ± 1.1	132.563	5.3 ± 1.1	133.063	5.3 ± 1.1	133.563	5.2 ± 1.0
134.063	5.0 ± 1.0	134.563	5.0 ± 1.0	135.063	5.0 ± 1.0	135.563	5.0 ± 1.0
136.063	5.0 ± 1.0	136.563	4.9 ± 1.0	137.063	5.0 ± 1.0	137.563	5.0 ± 1.0
138.063	4.9 ± 1.0	138.563	4.9 ± 1.0	139.063	5.1 ± 1.0	139.563	4.9 ± 1.0
140.063	4.9 ± 1.0	140.563	4.9 ± 1.0	141.063	4.8 ± 1.0	141.563	5.0 ± 1.0
142.063	4.8 ± 1.0	142.563	4.8 ± 1.0	143.063	4.8 ± 1.0	143.563	4.8 ± 1.0
144.063	4.9 ± 1.0	144.563	4.8 ± 1.0	145.563	4.6 ± 0.9	146.063	4.6 ± 0.9
146.563	4.6 ± 0.9	147.063	4.6 ± 0.9	147.563	4.6 ± 0.9	148.063	4.6 ± 0.9
148.563	4.6 ± 0.9	149.063	4.5 ± 0.9	149.563	4.5 ± 0.9	150.063	4.5 ± 0.9

(Table continued)

TABLE IV. *(Continued)*

f (Hz)	$h_0^{90\%} \times 10^{25}$	f (Hz)	$h_0^{90\%} \times 10^{25}$	f (Hz)	$h_0^{90\%} \times 10^{25}$	f (Hz)	$h_0^{90\%} \times 10^{25}$
150.563	4.5 ± 0.9	151.063	4.5 ± 0.9	151.563	4.5 ± 0.9	152.063	4.5 ± 0.9
152.563	4.5 ± 0.9	153.063	4.6 ± 0.9	153.563	4.5 ± 0.9	154.063	4.5 ± 0.9
154.563	4.5 ± 0.9	155.063	4.6 ± 0.9	155.563	4.5 ± 0.9	156.063	4.5 ± 0.9
156.563	4.5 ± 0.9	157.063	4.5 ± 0.9	157.563	4.5 ± 0.9	158.063	4.5 ± 0.9
158.563	4.5 ± 0.9	159.063	4.5 ± 0.9	159.563	4.4 ± 0.9	160.063	4.4 ± 0.9
160.563	4.5 ± 0.9	161.063	4.5 ± 0.9	161.563	4.4 ± 0.9	162.063	4.5 ± 0.9
162.563	4.5 ± 0.9	163.063	4.5 ± 0.9	163.563	4.5 ± 0.9	164.063	4.4 ± 0.9
164.563	4.4 ± 0.9	165.063	4.4 ± 0.9	165.563	4.4 ± 0.9	166.063	4.4 ± 0.9
166.563	4.4 ± 0.9	167.063	4.4 ± 0.9	167.563	4.4 ± 0.9	168.063	4.3 ± 0.9
168.563	4.3 ± 0.9	169.063	4.3 ± 0.9	169.563	4.3 ± 0.9	170.063	4.3 ± 0.9
170.563	4.3 ± 0.9	171.063	4.3 ± 0.9	171.563	4.3 ± 0.9	172.063	4.3 ± 0.9
172.563	4.3 ± 0.9	173.063	4.3 ± 0.9	173.563	4.3 ± 0.9	174.063	4.4 ± 0.9
174.563	4.3 ± 0.9	175.063	4.4 ± 0.9	175.563	4.4 ± 0.9	176.063	4.8 ± 1.0
176.563	5.0 ± 1.0	177.063	5.0 ± 1.0	177.563	5.0 ± 1.0	178.063	5.1 ± 1.0
178.563	5.6 ± 1.1	181.063	5.7 ± 1.1	181.563	5.3 ± 1.1	182.063	5.3 ± 1.1
182.563	5.4 ± 1.1	183.063	5.2 ± 1.0	183.563	4.9 ± 1.0	184.063	5.1 ± 1.0
184.563	4.8 ± 1.0	185.063	5.0 ± 1.0	185.563	4.9 ± 1.0	186.063	4.9 ± 1.0
186.563	4.8 ± 1.0	187.063	4.8 ± 1.0	187.563	5.0 ± 1.0	188.063	5.3 ± 1.1
188.563	5.3 ± 1.1	189.063	6.3 ± 1.3	189.563	6.1 ± 1.2	190.063	5.5 ± 1.1
190.563	5.1 ± 1.0	191.063	4.8 ± 1.0	191.563	4.8 ± 1.0	192.063	4.8 ± 1.0
192.563	4.8 ± 1.0	193.063	4.6 ± 0.9	193.563	4.5 ± 0.9	194.063	4.7 ± 0.9
194.563	4.5 ± 0.9	195.063	4.8 ± 1.0	195.563	4.9 ± 1.0	196.063	5.1 ± 1.0
196.563	5.0 ± 1.0	197.063	4.9 ± 1.0	197.563	5.2 ± 1.0	198.063	5.3 ± 1.1
198.563	5.3 ± 1.1	199.063	6.2 ± 1.2	199.563	6.7 ± 1.3	200.063	5.6 ± 1.1
200.563	5.7 ± 1.1	201.063	5.9 ± 1.2	201.563	5.3 ± 1.1	202.063	5.3 ± 1.1
202.563	5.4 ± 1.1	203.063	4.9 ± 1.0	203.563	4.5 ± 0.9	204.063	4.4 ± 0.9
204.563	4.4 ± 0.9	205.063	4.4 ± 0.9	205.563	4.5 ± 0.9	206.063	4.4 ± 0.9
206.563	4.5 ± 0.9	207.063	4.6 ± 0.9	207.563	4.6 ± 0.9	208.063	4.9 ± 1.0
208.563	5.1 ± 1.0	209.063	5.0 ± 1.0	209.563	5.1 ± 1.0	210.063	5.1 ± 1.0
210.563	4.6 ± 0.9	211.063	4.6 ± 0.9	211.563	4.5 ± 0.9	212.063	4.4 ± 0.9
212.563	4.4 ± 0.9	213.063	4.5 ± 0.9	213.563	4.5 ± 0.9	214.063	4.3 ± 0.9
214.563	4.4 ± 0.9	215.063	4.4 ± 0.9	215.563	4.3 ± 0.9	216.063	4.3 ± 0.9
216.563	4.3 ± 0.9	217.063	4.3 ± 0.9	217.563	4.3 ± 0.9	218.063	4.3 ± 0.9
218.563	4.3 ± 0.9	219.063	4.4 ± 0.9	219.563	4.3 ± 0.9	220.063	4.4 ± 0.9
220.563	4.4 ± 0.9	221.063	4.4 ± 0.9	221.563	4.4 ± 0.9	222.063	4.5 ± 0.9
222.563	4.6 ± 0.9	223.063	4.7 ± 0.9	223.563	4.8 ± 1.0	224.063	4.7 ± 0.9
224.563	4.6 ± 0.9	225.063	4.6 ± 0.9	225.563	4.6 ± 0.9	226.063	4.5 ± 0.9
226.563	4.5 ± 0.9	227.063	4.5 ± 0.9	227.563	4.5 ± 0.9	228.063	4.5 ± 0.9
228.563	4.6 ± 0.9	229.063	4.6 ± 0.9	229.563	4.6 ± 0.9	230.063	4.9 ± 1.0
230.563	4.6 ± 0.9	231.063	4.6 ± 0.9	231.563	4.6 ± 0.9	232.063	4.5 ± 0.9
232.563	4.6 ± 0.9	233.063	4.7 ± 0.9	233.563	4.8 ± 1.0	234.063	4.7 ± 0.9
234.563	4.6 ± 0.9	235.063	4.6 ± 0.9	235.563	4.6 ± 0.9	236.063	4.5 ± 0.9
236.563	4.5 ± 0.9	237.063	4.5 ± 0.9	237.563	4.5 ± 0.9	238.063	4.5 ± 0.9
238.563	4.5 ± 0.9	240.563	4.6 ± 0.9	241.063	4.6 ± 0.9	241.563	4.7 ± 0.9
242.063	4.6 ± 0.9	242.563	4.5 ± 0.9	243.063	4.7 ± 0.9	243.563	4.7 ± 0.9
244.063	4.5 ± 0.9	244.563	4.5 ± 0.9	245.063	4.5 ± 0.9	245.563	4.6 ± 0.9
246.063	4.6 ± 0.9	246.563	4.6 ± 0.9	247.063	4.6 ± 0.9	247.563	4.6 ± 0.9
248.063	4.6 ± 0.9	248.563	4.7 ± 0.9	249.063	4.7 ± 0.9	249.563	4.6 ± 0.9
250.063	4.6 ± 0.9	250.563	4.6 ± 0.9	251.063	4.6 ± 0.9	251.563	4.6 ± 0.9
252.063	4.6 ± 0.9	252.563	4.6 ± 0.9	253.063	4.6 ± 0.9	253.563	4.6 ± 0.9
254.063	4.6 ± 0.9	254.563	4.6 ± 0.9	255.063	4.6 ± 0.9	255.563	4.8 ± 1.0
256.063	4.7 ± 0.9	256.563	4.7 ± 0.9	257.063	5.2 ± 1.0	257.563	4.8 ± 1.0
258.063	4.9 ± 1.0	258.563	4.8 ± 1.0	259.063	4.7 ± 0.9	259.563	4.7 ± 0.9
260.063	4.7 ± 0.9	260.563	4.7 ± 0.9	261.063	4.7 ± 0.9	261.563	4.7 ± 0.9
262.063	4.7 ± 0.9	262.563	4.7 ± 0.9	263.063	4.7 ± 0.9	263.563	4.7 ± 0.9

(Table continued)

TABLE IV. *(Continued)*

f (Hz)	$h_0^{90\%} \times 10^{25}$	f (Hz)	$h_0^{90\%} \times 10^{25}$	f (Hz)	$h_0^{90\%} \times 10^{25}$	f (Hz)	$h_0^{90\%} \times 10^{25}$
264.063	4.8 ± 1.0	264.563	4.8 ± 1.0	265.063	4.8 ± 1.0	265.563	4.8 ± 1.0
266.063	4.8 ± 1.0	266.563	4.8 ± 1.0	267.063	4.8 ± 1.0	267.563	5.0 ± 1.0
268.063	5.0 ± 1.0	268.563	4.9 ± 1.0	269.063	4.9 ± 1.0	269.563	4.9 ± 1.0
270.063	5.1 ± 1.0	270.563	5.2 ± 1.0	271.063	5.0 ± 1.0	271.563	5.0 ± 1.0
272.063	4.9 ± 1.0	272.563	4.9 ± 1.0	273.063	5.0 ± 1.0	273.563	5.0 ± 1.0
274.063	4.9 ± 1.0	274.563	4.9 ± 1.0	275.063	4.9 ± 1.0	275.563	5.0 ± 1.0
276.063	5.3 ± 1.1	276.563	5.1 ± 1.0	277.063	5.1 ± 1.0	277.563	5.2 ± 1.0
278.063	5.2 ± 1.0	278.563	5.2 ± 1.0	279.063	5.4 ± 1.1	279.563	5.7 ± 1.1
280.063	5.5 ± 1.1	280.563	5.4 ± 1.1	281.063	5.3 ± 1.1	281.563	5.6 ± 1.1
282.063	5.4 ± 1.1	282.563	5.3 ± 1.1	283.063	5.3 ± 1.1	283.563	5.5 ± 1.1
284.063	5.2 ± 1.0	284.563	5.2 ± 1.0	285.063	5.2 ± 1.0	285.563	5.1 ± 1.0
286.063	5.1 ± 1.0	286.563	5.2 ± 1.0	287.063	5.2 ± 1.0	287.563	5.2 ± 1.0
288.063	5.2 ± 1.0	288.563	5.3 ± 1.1	289.063	5.2 ± 1.0	289.563	5.2 ± 1.0
290.063	5.2 ± 1.0	290.563	5.2 ± 1.0	291.063	5.2 ± 1.0	291.563	5.2 ± 1.0
292.063	5.2 ± 1.0	292.563	5.2 ± 1.0	293.063	5.2 ± 1.0	293.563	5.2 ± 1.0
294.063	5.3 ± 1.1	294.563	5.2 ± 1.0	295.063	5.2 ± 1.0	295.563	5.2 ± 1.0
296.063	5.2 ± 1.0	296.563	5.3 ± 1.1	297.063	5.3 ± 1.1	297.563	5.3 ± 1.1
298.063	5.3 ± 1.1	298.563	5.3 ± 1.1	300.563	5.4 ± 1.1	301.063	5.4 ± 1.1
301.563	5.4 ± 1.1	302.063	5.5 ± 1.1	302.563	5.4 ± 1.1	303.063	5.5 ± 1.1
303.563	5.6 ± 1.1	304.063	5.5 ± 1.1	304.563	5.4 ± 1.1	305.063	5.5 ± 1.1
305.563	5.5 ± 1.1	306.063	5.6 ± 1.1	306.563	5.6 ± 1.1	307.063	5.5 ± 1.1
307.563	5.5 ± 1.1	308.063	5.5 ± 1.1	308.563	5.6 ± 1.1	309.063	5.7 ± 1.1
309.563	5.8 ± 1.2	310.063	5.7 ± 1.1	310.563	5.7 ± 1.1	311.063	5.7 ± 1.1
311.563	5.9 ± 1.2	312.063	5.8 ± 1.2	312.563	5.7 ± 1.1	313.063	5.7 ± 1.1
313.563	5.8 ± 1.2	314.063	5.8 ± 1.2	314.563	5.7 ± 1.1	315.063	5.8 ± 1.2
315.563	5.8 ± 1.2	316.063	5.9 ± 1.2	316.563	6.1 ± 1.2	317.063	6.0 ± 1.2
317.563	5.9 ± 1.2	318.063	6.0 ± 1.2	318.563	6.0 ± 1.2	319.063	6.0 ± 1.2
319.563	6.0 ± 1.2	320.063	6.0 ± 1.2	320.563	6.1 ± 1.2	321.063	6.2 ± 1.2
321.563	6.3 ± 1.3	322.063	6.6 ± 1.3	322.563	6.5 ± 1.3	323.063	6.8 ± 1.4
323.563	6.9 ± 1.4	324.063	7.0 ± 1.4	324.563	6.8 ± 1.4	325.063	6.9 ± 1.4
325.563	7.0 ± 1.4	326.063	7.2 ± 1.4	326.563	7.6 ± 1.5	327.063	7.9 ± 1.6
327.563	7.9 ± 1.6	328.063	7.8 ± 1.6	328.563	7.7 ± 1.5	329.063	7.5 ± 1.5
329.563	7.4 ± 1.5	330.063	7.7 ± 1.5	330.563	7.9 ± 1.6	331.063	7.7 ± 1.5
331.563	8.0 ± 1.6	332.063	8.0 ± 1.6	332.563	8.0 ± 1.6	333.063	8.1 ± 1.6
333.563	8.5 ± 1.7	334.063	9.1 ± 1.8	334.563	10.2 ± 2.0	335.063	11.0 ± 2.2
335.563	10.8 ± 2.2	336.063	10.8 ± 2.2	336.563	10.8 ± 2.2	337.063	10.9 ± 2.2
337.563	11.1 ± 2.2	338.063	11.6 ± 2.3	338.563	12.4 ± 2.5	339.063	13.4 ± 2.7
350.563	15.1 ± 3.0	351.063	13.6 ± 2.7	351.563	12.7 ± 2.5	352.063	12.9 ± 2.6
352.563	12.0 ± 2.4	353.063	12.1 ± 2.4	353.563	12.6 ± 2.5	354.063	11.3 ± 2.3
354.563	11.3 ± 2.3	355.063	13.1 ± 2.6	355.563	14.8 ± 3.0	356.063	14.4 ± 2.9
356.563	12.4 ± 2.5	357.063	10.2 ± 2.0	357.563	9.1 ± 1.8	358.063	9.4 ± 1.9
358.563	8.8 ± 1.8	361.063	7.6 ± 1.5	361.563	7.3 ± 1.5	362.063	7.2 ± 1.4
362.563	7.2 ± 1.4	363.063	8.1 ± 1.6	363.563	8.3 ± 1.7	364.063	8.2 ± 1.6
364.563	8.4 ± 1.7	365.063	7.1 ± 1.4	365.563	6.9 ± 1.4	366.063	7.0 ± 1.4
366.563	6.9 ± 1.4	367.063	7.2 ± 1.4	367.563	7.1 ± 1.4	368.063	6.8 ± 1.4
368.563	6.9 ± 1.4	369.063	6.7 ± 1.3	369.563	7.0 ± 1.4	370.063	7.1 ± 1.4
370.563	6.9 ± 1.4	371.063	7.5 ± 1.5	371.563	6.8 ± 1.4	372.063	6.4 ± 1.3
372.563	6.4 ± 1.3	373.063	6.5 ± 1.3	373.563	6.9 ± 1.4	374.063	7.3 ± 1.5
374.563	6.9 ± 1.4	375.063	7.2 ± 1.4	375.563	6.8 ± 1.4	376.063	6.7 ± 1.3
376.563	6.8 ± 1.4	377.063	7.7 ± 1.5	377.563	8.3 ± 1.7	378.063	7.1 ± 1.4
378.563	6.6 ± 1.3	379.063	6.5 ± 1.3	379.563	6.6 ± 1.3	380.063	6.6 ± 1.3
380.563	6.5 ± 1.3	381.063	6.6 ± 1.3	381.563	6.7 ± 1.3	382.063	6.8 ± 1.4
382.563	7.0 ± 1.4	383.063	7.3 ± 1.5	383.563	7.2 ± 1.4	384.063	7.4 ± 1.5
384.563	7.8 ± 1.6	385.063	8.1 ± 1.6	385.563	9.3 ± 1.9	386.063	8.9 ± 1.8
386.563	7.4 ± 1.5	387.063	7.0 ± 1.4	387.563	6.8 ± 1.4	388.063	6.9 ± 1.4

(Table continued)

TABLE IV. *(Continued)*

f (Hz)	$h_0^{90\%} \times 10^{25}$	f (Hz)	$h_0^{90\%} \times 10^{25}$	f (Hz)	$h_0^{90\%} \times 10^{25}$	f (Hz)	$h_0^{90\%} \times 10^{25}$
388.563	7.4 ± 1.5	389.063	6.9 ± 1.4	389.563	6.6 ± 1.3	390.063	6.5 ± 1.3
390.563	6.8 ± 1.4	391.063	7.0 ± 1.4	391.563	6.8 ± 1.4	392.063	6.6 ± 1.3
392.563	6.6 ± 1.3	393.063	6.6 ± 1.3	393.563	6.5 ± 1.3	394.063	6.5 ± 1.3
394.563	6.4 ± 1.3	395.063	6.5 ± 1.3	395.563	7.1 ± 1.4	396.063	6.8 ± 1.4
396.563	6.6 ± 1.3	397.063	6.6 ± 1.3	397.563	6.4 ± 1.3	398.063	6.4 ± 1.3
398.563	6.6 ± 1.3	399.063	6.6 ± 1.3	399.563	6.7 ± 1.3	400.563	6.6 ± 1.3
401.063	6.4 ± 1.3	401.563	6.4 ± 1.3	402.063	6.4 ± 1.3	402.563	6.4 ± 1.3
403.063	6.7 ± 1.3	403.563	6.8 ± 1.4	404.063	6.7 ± 1.3	404.563	6.5 ± 1.3
405.063	6.4 ± 1.3	405.563	6.6 ± 1.3	406.063	6.7 ± 1.3	406.563	6.5 ± 1.3
407.063	6.4 ± 1.3	407.563	6.4 ± 1.3	408.063	6.4 ± 1.3	408.563	6.5 ± 1.3
409.063	6.5 ± 1.3	409.563	6.4 ± 1.3	410.063	6.4 ± 1.3	410.563	6.5 ± 1.3
411.063	6.6 ± 1.3	411.563	6.6 ± 1.3	412.063	6.7 ± 1.3	412.563	7.0 ± 1.4
413.063	6.6 ± 1.3	413.563	6.6 ± 1.3	414.063	6.6 ± 1.3	414.563	6.7 ± 1.3
415.063	6.5 ± 1.3	415.563	6.5 ± 1.3	416.063	6.5 ± 1.3	416.563	6.7 ± 1.3
417.063	6.7 ± 1.3	417.563	6.6 ± 1.3	418.063	6.5 ± 1.3	418.563	6.6 ± 1.3
420.563	6.7 ± 1.3	421.063	6.7 ± 1.3	421.563	6.8 ± 1.4	422.063	7.0 ± 1.4
422.563	7.7 ± 1.5	423.063	7.0 ± 1.4	423.563	6.9 ± 1.4	424.063	6.9 ± 1.4
424.563	7.0 ± 1.4	425.063	7.3 ± 1.5	425.563	7.7 ± 1.5	426.063	7.8 ± 1.6
426.563	7.8 ± 1.6	427.063	7.8 ± 1.6	427.563	8.3 ± 1.7	428.063	8.8 ± 1.8
428.563	9.7 ± 1.9	429.063	9.7 ± 1.9	429.563	8.2 ± 1.6	430.063	8.2 ± 1.6
430.563	7.9 ± 1.6	431.063	8.3 ± 1.7	431.563	9.4 ± 1.9	432.063	8.3 ± 1.7
432.563	7.8 ± 1.6	433.063	7.2 ± 1.4	433.563	6.9 ± 1.4	434.063	6.9 ± 1.4
434.563	6.9 ± 1.4	435.063	6.9 ± 1.4	435.563	6.7 ± 1.3	436.063	6.7 ± 1.3
436.563	6.9 ± 1.4	437.063	6.9 ± 1.4	437.563	6.7 ± 1.3	438.063	6.9 ± 1.4
438.563	6.8 ± 1.4	439.063	7.0 ± 1.4	439.563	7.0 ± 1.4	440.063	6.9 ± 1.4
440.563	6.9 ± 1.4	441.063	7.1 ± 1.4	441.563	6.8 ± 1.4	442.063	6.8 ± 1.4
442.563	6.8 ± 1.4	443.063	6.8 ± 1.4	443.563	6.8 ± 1.4	444.063	6.8 ± 1.4
444.563	6.8 ± 1.4	445.063	6.8 ± 1.4	445.563	6.9 ± 1.4	446.063	6.9 ± 1.4
446.563	7.2 ± 1.4	447.063	7.0 ± 1.4	447.563	7.1 ± 1.4	448.063	7.1 ± 1.4
448.563	7.3 ± 1.5	449.063	7.2 ± 1.4	449.563	7.0 ± 1.4	450.063	7.0 ± 1.4
450.563	7.4 ± 1.5	451.063	7.2 ± 1.4	451.563	7.3 ± 1.5	452.063	7.3 ± 1.5
452.563	7.2 ± 1.4	453.063	7.2 ± 1.4	453.563	7.2 ± 1.4	454.063	7.4 ± 1.5
454.563	8.2 ± 1.6	455.063	7.3 ± 1.5	455.563	7.4 ± 1.5	456.063	7.5 ± 1.5
456.563	7.2 ± 1.4	457.063	7.1 ± 1.4	457.563	7.0 ± 1.4	458.063	7.0 ± 1.4
458.563	7.0 ± 1.4	459.063	7.0 ± 1.4	459.563	7.0 ± 1.4	460.063	7.0 ± 1.4
460.563	7.2 ± 1.4	461.063	7.2 ± 1.4	461.563	7.1 ± 1.4	462.063	7.1 ± 1.4
462.563	7.2 ± 1.4	463.063	7.2 ± 1.4	463.563	7.2 ± 1.4	464.063	7.2 ± 1.4
464.563	7.3 ± 1.5	465.063	7.8 ± 1.6	465.563	8.1 ± 1.6	466.063	7.8 ± 1.6
466.563	7.8 ± 1.6	467.063	7.7 ± 1.5	467.563	8.0 ± 1.6	468.063	7.5 ± 1.5
468.563	7.4 ± 1.5	469.063	7.4 ± 1.5	469.563	7.4 ± 1.5	470.063	7.7 ± 1.5
470.563	7.7 ± 1.5	471.063	7.9 ± 1.6	471.563	8.1 ± 1.6	472.063	7.7 ± 1.5
472.563	7.6 ± 1.5	473.063	7.9 ± 1.6	473.563	7.8 ± 1.6	474.063	7.6 ± 1.5
474.563	7.7 ± 1.5	475.063	7.7 ± 1.5	475.563	8.0 ± 1.6	476.063	7.7 ± 1.5
476.563	7.5 ± 1.5	477.063	7.7 ± 1.5	477.563	7.7 ± 1.5	478.063	7.5 ± 1.5
478.563	7.5 ± 1.5	480.563	7.6 ± 1.5	481.063	7.6 ± 1.5	481.563	7.7 ± 1.5
482.063	7.6 ± 1.5	482.563	7.6 ± 1.5	483.063	7.7 ± 1.5	483.563	7.6 ± 1.5
484.063	7.6 ± 1.5	484.563	7.6 ± 1.5	485.063	7.6 ± 1.5	485.563	7.5 ± 1.5
486.063	7.5 ± 1.5	486.563	7.5 ± 1.5	487.063	7.5 ± 1.5	487.563	7.5 ± 1.5
488.063	7.5 ± 1.5	488.563	7.6 ± 1.5	489.063	7.7 ± 1.5	489.563	8.2 ± 1.6
490.063	8.3 ± 1.7	490.563	7.9 ± 1.6	491.063	7.9 ± 1.6	491.563	8.0 ± 1.6
492.063	8.1 ± 1.6	492.563	8.2 ± 1.6	493.063	8.5 ± 1.7	493.563	9.2 ± 1.8
494.063	9.9 ± 2.0	494.563	9.0 ± 1.8	495.063	9.6 ± 1.9	495.563	8.7 ± 1.7
496.063	8.1 ± 1.6	496.563	8.0 ± 1.6	497.063	8.0 ± 1.6	497.563	8.1 ± 1.6
498.063	7.8 ± 1.6	498.563	7.7 ± 1.5	499.063	7.7 ± 1.5	499.563	7.8 ± 1.6
500.063	8.1 ± 1.6	500.563	7.7 ± 1.5	501.063	7.6 ± 1.5	501.563	7.6 ± 1.5

(Table continued)

TABLE IV. *(Continued)*

f (Hz)	$h_0^{90\%} \times 10^{25}$	f (Hz)	$h_0^{90\%} \times 10^{25}$	f (Hz)	$h_0^{90\%} \times 10^{25}$	f (Hz)	$h_0^{90\%} \times 10^{25}$
502.063	7.6 ± 1.5	502.563	7.6 ± 1.5	503.063	7.7 ± 1.5	503.563	7.6 ± 1.5
504.063	7.7 ± 1.5	504.563	7.8 ± 1.6	505.063	7.8 ± 1.6	505.563	7.8 ± 1.6
506.063	7.7 ± 1.5	506.563	7.7 ± 1.5	507.063	7.6 ± 1.5	507.563	7.6 ± 1.5
508.063	7.6 ± 1.5	508.563	7.6 ± 1.5	509.063	7.7 ± 1.5	509.563	7.8 ± 1.6

[1] B. P. Abbott *et al.* (LIGO Scientific Collaboration), Einstein@Home all-sky search for periodic gravitational waves in LIGO S5 data, Phys. Rev. D **87**, 042001 (2013).

[2] M. Shaltev, P. Leaci, M. A. Papa, and R. Prix, Fully coherent follow-up of continuous gravitational-wave candidates: an application to Einstein@Home results, Phys. Rev. D **89**, 124030 (2014).

[3] J. Aasi *et al.* (LIGO Scientific and VIRGO Collaborations), Directed search for continuous gravitational waves from the Galactic center, Phys. Rev. D **88**, 102002 (2013).

[4] B. Behnke, M. A. Papa, and R. Prix, Postprocessing methods used in the search for continuous gravitational-wave signals from the Galactic Center, Phys. Rev. D **91**, 064007 (2015).

[5] B. P. Abbott *et al.* (LIGO Scientific and Virgo Collaborations), Results of the deepest all-sky survey for continuous gravitational waves on LIGO S6 data running on the Einstein@Home volunteer distributed computing project, Phys. Rev. D **94**, 102002 (2016)..

[6] H. J. Pletsch, Parameter-space correlations of the optimal statistic for continuous gravitational-wave detection, Phys. Rev. D **78**, 102005 (2008).

[7] H. J. Pletsch, Parameter-space metric of semicoherent searches for continuous gravitational waves, Phys. Rev. D **82**, 042002 (2010).

[8] https://www.einsteinathome.org/.

[9] http://www.aei.mpg.de/24838/02_Computing_and_ATLAS.

[10] A. Singh, M. A. Papa, H.-B. Eggenstein, S. Zhu, H. Pletsch, B. Allen, O. Bock, B. Maschenchalk, R. Prix, and X. Siemens, Results of an all-sky high-frequency Einstein@Home search for continuous gravitational waves in LIGO 5th Science Run, Phys. Rev. D **94**, 064061 (2016).

[11] D. Keitel, R. Prix, M. A. Papa, P. Leaci, and M. Siddiqi, Search for continuous gravitational waves: Improving robustness versus instrumental artifacts, Phys. Rev. D **89**, 064023 (2014).

[12] J. Aasi *et al.* (LIGO Collaboration), Searches for continuous gravitational waves from nine young supernova remnants, Astrophys. J. **813**, 39 (2015).

[13] B. P. Abbott *et al.* (LIGO Scientific and Virgo Collaborations), Comprehensive all-sky search for periodic gravitational waves in the sixth science run LIGO data, Phys. Rev. D **94**, 042002 (2016).

[14] J. Aasi *et al.* (LIGO Scientific and VIRGO Collaborations), First low frequency all-sky search for continuous gravitational wave signals, Phys. Rev. D **93**, 042007 (2016).

[15] N. K. Johnson-McDaniel and B. J. Owen, Maximum elastic deformations of relativistic stars, Phys. Rev. D **88**, 044004 (2013).

[16] S. Walsh *et al.*, Comparison of methods for the detection of gravitational waves from unknown neutron stars, Phys. Rev. D **94**, 124010 (2016).

[17] K. Wette, Empirically extending the range of validity of parameter-space metrics for all-sky searches for gravitational-wave pulsars, arXiv:1607.00241.

[18] K. Wette, Parameter-space metric for all-sky semicoherent searches for gravitational-wave pulsars, Phys. Rev. D **92**, 082003 (2015).

[19] K. Wette, Lattice template placement for coherent all-sky searches for gravitational-wave pulsars, Phys. Rev. D **90**, 122010 (2014).

[20] K. Wette and R. Prix, Flat parameter-space metric for all-sky searches for gravitational-wave pulsars, Phys. Rev. D **88**, 123005 (2013).

[21] S. J. Zhu *et al.*, An Einstein@home search for continuous gravitational waves from Cassiopeia A, Phys. Rev. D **94**, 082008 (2016).